Journal of Cleaner Production 308 (2021) 127385

Contents lists available at ScienceDirect

Journal of Cleaner Production

journal homepage: www.elsevier.com/locate/jclepro

Improving degradation of real wastewaters with self-heating magnetic nanocatalysts

Alvaro Gallo-Cordova [a,b,*], Juan José Castro [b], Elin L. Winkler [c], Enio Lima Jr. [c], Roberto D. Zysler [c], María del Puerto Morales [a], Jesús G. Ovejero [a,**], Daniela Almeida Streitwieser [b]

[a] Instituto de Ciencia de Materiales de Madrid, ICMM/CSIC, C/Sor Juana Inés de la Cruz 3, 28049, Madrid, Spain
[b] Instituto para el Desarrollo de Energías y Materiales Alternativos, IDEMA, Departamento de Ingeniería Química, Universidad San Francisco de Quito USFQ, EC 170901 Quito, Ecuador
[c] Instituto de Nanociencia y Nanotecnología, CNEA, CONICET, Centro Atómico Bariloche, 8400 S. C. Bariloche, Argentina

ARTICLE INFO

Handling editor: Bin Chen

Keywords:
Iron oxide nanoparticles
Advanced oxidation
Reactive oxygen species
Leachate treatment
Organic dyes
Wastewater treatment

ABSTRACT

Industrial effluents contain a wide range of organic pollutants that present harmful effects on the environment and deprived communities with no access to clean water. As this organic matter is resistant to conventional treatments, Advanced Oxidation Processes (AOPs) have emerged as a suitable option to counteract these environmental challenges. Engineered iron oxide nanoparticles have been widely tested in AOPs catalysis, but their full potential as magnetic induction self-heating catalysts has not been studied yet on real and highly contaminated industrial wastewaters. In this study we have designed a self-heating catalyst with a finely tuned structure of small cores (10 nm) aggregates to develop multicore particles (40 nm) with high magnetic moment and high colloidal stability. This nanocatalyst, that can be separated by magnetic harvesting, is able to increase reaction temperatures (up to 90 °C at 1 mg/mL suspension in 5 min) under the action of alternating magnetic fields. This efficient heating was tested in the degradation of a model compound (methyl orange) and real wastewaters, such as leachate from a solid landfill (LIX) and colored wastewater from a textile industry (TIW). It was possible to increase reaction rates leading to a reduction of the chemical oxygen demand of 50 and 90%, for TIW and LIX. These high removal and degradation ability of the magnetic nanocatalyst was sustained with the formation of strong reactive oxygen species by a Fenton-like mechanism as proved by electron paramagnetic resonance. These findings represent an important advance for the industrial implementation of a scalable, non-toxic, self-heating catalysts that can certainly enhance AOP for wastewater treatment in a more sustainable and efficient way.

1. Introduction

The rapid industrialization of developing countries has generated crucial challenges dealing with environmental pollution. There is a huge generation of industrial solid wastes that ends up in solid landfills and eventually in different waterbodies in the form of leachates, similar issues occurs with polluted effluents from a large list of industrial activities (Khandelwal et al., 2019). The great diversity of compounds in solid landfill leachates and the mixture of hazardous dyes in textiles wastewaters restrict the efficiency of the most common treatment techniques (Oulego et al., 2016) and new ones. The use of engineered metal oxides nanoparticles have emerged as promising agents for full scale environmental remediation (Adeleye et al., 2016). Among them, iron oxide nanoparticles present unique properties for the development of magnetic separation and degradation strategies that compensate the effects of the huge generation of industrial solid wastes and polluted effluents (Gutierrez et al., 2017; Xu et al., 2012).

In solid landfills, the humidity of solid wastes and the rainwater that percolates through them generate a highly polluting wastewater by reacting with the decomposing products of the organic matter (Kjeldsen et al., 2002). These strongly colored and odorous leachates present a variable composition that depends on the environmental conditions, the type of waste deposited in the landfill, and the age of the leachate (Oulego et al., 2016; Renou et al., 2008). The diversity of pollutants in

* Corresponding author. Instituto de Ciencia de Materiales de Madrid, ICMM/CSIC, C/Sor Juana Inés de la Cruz 3, 28049, Madrid, Spain.
** Corresponding author.
E-mail addresses: alvaro.gallo@csic.es (A. Gallo-Cordova), jesus.g.ovejero@csic.es (J.G. Ovejero).

https://doi.org/10.1016/j.jclepro.2021.127385
Received 30 October 2020; Received in revised form 24 March 2021; Accepted 2 May 2021
Available online 8 May 2021

this kind of wastewater makes their treatment process complicated, variable and expensive. In most solid landfills, the leachates are stored in different deposits for its later treatment that can involve a combination of biological, physical and chemical processes like aerobic or anaerobic treatment, coagulation/flocculation, ultrafiltration and inverse osmosis, among others (Miao et al., 2019; Renou et al., 2008). Another common pollutants are the organic dyes coming from different industries such as production of fabrics and textiles (Madhav et al., 2018; Saini, 2017). These highly colored wastes are not only a threat to human health but also to environment, causing obstruction of light and interfering with biological processes within the stream ecosystem (Tkaczyk et al., 2020). A common industrial solution to remove these kind of dyes is using biological treatments (Kong et al., 2019), adsorption or electrochemical methods (Martínez-Huitle and Brillas, 2009), but these techniques usually present difficulties when the composition of the effluent is slightly changed (Grace Pavithra et al., 2019; Rai et al., 2005; Zhou et al., 2019).

An interesting approach to treat both kind of wastewater are the Advanced Oxidation Processes (AOP) that are increasingly implemented in industrial plants for the oxidation of organic molecules (Aramyan, 2017; Garrido-Cardenas et al., 2020; Miklos et al., 2018). AOPs are able to transform recalcitrant compounds in more biodegradable molecules that can be mineralized by microorganisms (Paździor et al., 2019). The oxidation intermediates in this kind of wastewaters tend to be more and more resistant to a complete degradation. It results very interesting to combine the already existing biological treatment with AOP such as Fenton based, ozone based,photocatalytic processes, among others (Gautam et al., 2019; Rosa et al., 2020; Usman et al., 2020). AOP systems take advantage of the highly oxidative hydroxyl radicals generated in the Fenton reaction of ferrous ions with hydrogen peroxide (Rekhate and Srivastava, 2020). During this reaction, ferric anions are produced and can also react with hydrogen peroxide in a Fenton-like reaction. The radical species formed during Fenton and Fenton-like reactions, usually known as reactive oxygen species, have the effective oxidative ability to degrade organic pollutants by hydrogen abstraction, electron transferring, radical addition and/or combination (He et al., 2016; Wang, 2008). For industrial AOP, it is important to consider that these radicals with very short lifetime need to be generated in situ with the help of oxidizing agents, irradiation or with a catalyst. (Augugliaro et al., 2006; Gautam et al., 2019; Usman et al., 2020). Some of these methods implicate drawbacks that may limit their use on an industrial sustainable scale, *e.g.* the use of ultraviolet radiation that presents low photon efficiency being only about 5% of sunlight (Gehrke et al., 2015).

The use of magnetic iron oxide nanoparticles for AOPs has been previously studied due to their low toxicity (Gallo-Cordova et al., 2021; Malhotra et al., 2020), iron ions availability, high surface area/volume ratios and their simple magnetic separation (Bethi et al., 2016; Hodges et al., 2018). Magnetite nanoparticles contain in their structure Fe^{2+} and Fe^{3+} ions that allow the continuous reactions of Haber-Weiss cycle (Rusevova et al., 2012). In this sense this kind of material has been already reported for the degradation of different organic compounds, but only few references use the particle selective heating capability under the influence of an alternating magnetic field (AMF) to support the degradation of the organic matter and none of them use real wastewaters (Chen et al., 2016; Munoz et al., 2020; Pirsaheb et al., 2019; Wydra et al., 2015). Besides the high specific surface area of the nanoparticles, which offers a high adsorption capacity for organic and inorganic compounds, they can be used as internal inductive heating sources with remarkable advantages against conventional methods (Yaqoob et al., 2020). In this type of heating, the high temperatures reached at the particle surface are reflected in higher reaction rates and in consequence, shorter residence times and lower production costs (Wang et al., 2019; Zaidi et al., 2014).

In previous works, we have shown already the capability of iron oxide nanoparticles to perform as an efficient adsorbent for organic and inorganic compounds from water, in particular for heavy metals such as lead and chromium and organic dyes like methyl orange (Gallo-Cordova et al, 2019, 2020). Here, we have developed a nanocatalyst consisting of uniform multicore iron oxide nanoparticles of 40 nm with aggregate cores of around 10 nm that are able not only to adsorb higher amounts of the organic matter but also degrade it by advanced oxidation processing and subsequent magnetic separation. The effect of heating the particles under an alternating magnetic field on the degradation of organic matter in water have been compared to experiments carried out at 25, 60 and 90 °C using a conventional thermal reactor. The degradation capacity of the catalyst has been tested with controlled preparations of methyl orange (MO) as a well-known organic pollutant, and with industrial leachate from the solid landfill of Quito City (LIX) and textile wastewater from a local industry (TIW). The magnetic separation feasibility of the magnetic catalyst has been analyzed by magnetophoresis analysis in a field gradient.

2. Materials and methods

2.1. Chemical reagents and analysis

Reagent such as Iron(II) chloride tetrahydrate ($FeCl_2{\cdot}4H_2O$, ≥99%), iron(III) chloride hexahydrate ($FeCl_3{\cdot}6H_2O$, ≥99%), sodium hydroxide (NaOH, ≥98%), diethylene glycol (DEG, 99%), N-Methyldiethanolamine (NMDEA, 99%), nitric acid (HNO_3, 65%), iron(III) nitrate nonahydrate ($Fe(NO_3)_3{\cdot}9H_2O$, 95%) ethanol (99.8%), ethyl acetate (99%), methyl orange (MO, 85%), sulfuric acid (H_2SO_4, 95%) were purchased form Sigma Aldrich. A high concentrated methyl orange stock solution (500 mg/L) was prepared and different aliquots at lower concentrations were prepared by dilution from the stock solution. MO was used as model compound for comparison purposes and its concentration was analyzed by ultraviolet–visible spectroscopy carried out in a Biochrom WPA Biowave DNA life science spectrophotometer at 503 nm (Ito and Yamamoto, 2015).

The landfill leachate (LIX) and textile industry wastewater (TIW) collected for the experimental procedure were taken from the solid landfill of Quito city and from a representative local textile industry. There was a 16 total sampling considering the international standard ISO 5667–3:2019 (ISO 5667–3:2019, 2019). All samples were carefully transported to the laboratory and kept under refrigeration at 4 °C for subsequent analyses. Table S1 summarizes a full description of this real wastewaters samples. Degradation and mineralization yield of the organic pollutants in the samples were traced by measuring the chemical oxygen demand (COD) and total organic carbon (TOC) using a DR890 HACH colorimeter at a 610 nm wavelength. For COD measurement the standard method of water and wastewater was followed (Rice et al., 2017). Briefly, a mixture of 2.5 mL of the sample with 3.5 mL of H_2SO_4 and 1.5 mL of the potassium dichromate standard (0.03 M) was previously digested at 150 °C in a DRB200 HACH reactor. For TOC determination, the HACH method 10173 using Test 'N Tube™ Vials was performed prior to the measurements (Hach Co, 1999). Hydrogen peroxide interference was controlled by using a blank with same concentration as the samples. The elemental composition of the samples was analyzed before and after catalytic degradation by coupled plasma optical emission spectroscopy (ICP-OES) in a PerkinElmer apparatus, OPTIME 2100DV.

2.2. Magnetic nanocatalyst synthesis

An optimized polyol method was used to synthesize the monodisperse magnetic iron oxide nanocatalyst (MNC) using iron chloride as iron precursor in an aminated polyol media (Ammar and Fiévet, 2020; Lartigue et al., 2012). Among the different methods reported for the preparation of multicore structures (table S2), we choose this one to obtain small multicore structures (<50 nm) with large cores to maximize heating capability and magnetophoretic mobility. For this, 96 g of the solvent media were prepared with DEG and NMDEA (50/50 w/w). A

mixture of 1.6 mmol of $FeCl_2{\cdot}4H_2O$ and 3.2 mmol of $FeCl_3{\cdot}6H_2O$ was added to 64 g of the solvent mixture and magnetically stirred at 1350 rpm for 45 min. Simultaneously, 12.8 mmol of NaOH were ultrasonic mixed in 32 g of the solvent mixture DEG and NMDEA (50/50 w/w) at 80 °C for 45 min. Afterwards, the NaOH solution was carefully poured onto the iron solution and stirred at 1350 rpm for another 45 min. The mixture was placed in a Teflon-lined reactor of 100-mL capacity and sealed in an autoclave. The reaction was left with no agitation at 220 °C for 16 h. The reactor product, cooled inside the oven, was recovered by magnetic separation. The supernatant was discarded, and the dark brown precipitate was washed several times with a mixture of ethanol and ethyl acetate, 50% in volume. This optimized procedure performed in a high-pressure autoclave is easily scalable which is an advantage for environmental industrial purposes. The polyol method presents the advantage of allowing the production of water dispersible particles prepared in solvents with high boiling points.

The MNC was subjected to an acidic treatment to improve the colloidal stability of the suspension and to assure oxidation of magnetite to maghemite and therefore, chemical stability for long time (Costo et al., 2015). Briefly, the obtained MNC was mechanically agitated with 10 mL of HNO_3 (10%) and then dispersed in 20 mL of distilled water. Then, 34 mmol of $Fe(NO_3)_3{\cdot}9H_2O$ was added, and the suspension was boiled under reflux for 45 min under stirring at 600 rpm. The sample was then cooled and treated with an additional 30 mL of HNO_3 for 10 min. The MNC were washed three times with distilled water and re-dispersed in 10 mL of pure (milliQ) water. The iron concentration of the suspension was measured by inductively coupled plasma optical emission spectroscopy (ICP-OES) in a PerkinElmer apparatus, OPTIME 2100DV, after acid digestion.

2.3. Magnetic nanocatalyst characterization

Morphological characteristics of the MNC (particle size, distribution and shape) were analyzed by transmission electron microscopy (TEM, JEOL JEM 1010 operated at 100 keV). The sample preparation consisted in placing a drop of the diluted MNC suspension on an amorphous carbon-coated copper grid and leaving it for evaporation at room temperature. Mean particle size and distribution were calculated by measuring around 200 particles (largest internal dimension) and fitting the data to a lognormal distribution.

X-Ray diffraction (XRD) was performed for phase identification and crystal structure of the iron oxide powder by using a diffractometer with a graphite monochromator (Bruker D8 Advance) and CuKα radiation (k = 1.5406 Å). The pattern was recorded within 20° and 70° (2Θ) and the mean crystal size was estimated from the full width at half-maximum of the greatest intensity peak (311) and the Scherrer's equation.

Thermal analysis (TGA/DSC) of the MNC was performed using a TA Instrument Q2000 differential scanning calorimeter. The MNC sample was heated up to 800 °C at 10 °C/min in air to measure the weight loss of DEG present in the nanoparticle surface (Rishikeshi et al., 2013). Fourier-transformed infrared spectroscopy in the range of 400–4000 $cm^{-1}$was used to detect the presence of amino groups and DEG rests in the MNC, using a Bruker IFS 66VS. Samples were prepared by mixing the MNC powder in KBr (2% w/w) and pressing them into pellets.

Magnetic properties of the MNC were analyzed in a vibrating sample magnetometer (MagLabVSM, 9T, Oxford Instrument). Samples were first dried at 50 °C overnight and then, pressed into the sample holder. Hysteresis loops were recorded at 290 K after applying a magnetic field up to ±2400 kA/m. Saturation magnetization (M_S) and remanent magnetization (M_R) values in $A.m^2/kg$ and coercivity (H_C) in kA/m were obtained. To measure how fast the MNC can be recovered in the presence of an external magnetic field gradient, the magnetophoretic mobility was studied as a function of time. This analysis was performed by measuring the turbidity of 500 mL of MNC suspension (0.05 mg_{Fe}/mL) under a horizontal magnetic field gradient of $\nabla H = 100$ T/m in a 2500 s time interval (Sepmag Q500 ML ©). A sample consisting on single core particles of 30 nm mean diameter, synthesized by prolonging the heating in the autoclave for 24 h, was used for comparison purposes.

Specific power absorption rate (SAR) of MNC in water was measured on a Fives Celes generator, model Nº 12118 M01 (France). This system is equipped with a water-cooled copper coil of 50 mm diameter with 6 turns. Experiments were performed with the sample placed in a vial in the middle of the heating coil under frequencies of 100 and 200 kHz at different external field amplitudes (from 8 to 40 kA/m). A schematic representation of the equipment and experimental set-up is detailed in Scheme 1. It can be highlighted the well-defined insulation over the inductor and the controlled environment with a thermostat ensuring that the heating is only coming from the MNC. The same experimental set-up was also used to perform the magnetic induction heating AOP on the wastewater samples.

SAR measurements were performed with at least 500 μL of the MNC suspension at 1 mg_{MNC}/mL, just after ultrasonic stirring for 5 min. The initial temperature was settled at 21 °C with the thermostat and temperature variation in the sample was measured using a fiber optic temperature sensor OSENSA's FTX. SAR value was obtained by using Equation S1.

The specific surface area of the MNC was also studied using a TriStar II 320 (Micrometrics) system through continuous recording of the nitrogen adsorbed into the MNC surface at different partial pressures and 77 K. The samples were degasified at 393 K and 0.1 mbar for 12 h. The MNC specific surface area and the pore size distribution were calculated using BET equation (Brunauer et al., 1938) and BJH method (Villarroel-Rocha et al., 2014).

2.4. Free radicals produced in the Fenton reaction

The Fenton activity was evaluated by Electron Paramagnetic Resonance spectroscopy (EPR) using the spintrap standard method (Davies, 2016; Eaton et al., 2010; Moreno Maldonado et al., 2019). The spin-traps are diamagnetic molecules that adduct the highly reactive free radicals and generate more stable paramagnetic species that can be identified and quantified by the EPR. The MNC Fenton activity was tested in a solution containing 120 μg of nanoparticles in 200 μL of an acetate buffer solution (0.01 M, pH = 5), and 50 μL of a solution of the standard spin-trap 5,5-dimethyl-1-pyrroline N-oxide (DMPO) in DMSO (0.33 g/mL). Finally, 10 μL of 30% H_2O_2 was added, which started the reaction, and is considered the initial time for the spectra collected. The EPR equipment is an ELEXSYS II-E500 spectrometer (Bruker), having an X-band resonant cavity (9.4 GHz). The spectra were acquired at 24 ± 1 °C at different times until 60 min, with an attenuation of 10 dB (20 mW microwave power) and a modulation field of 1 Oe of amplitude. To

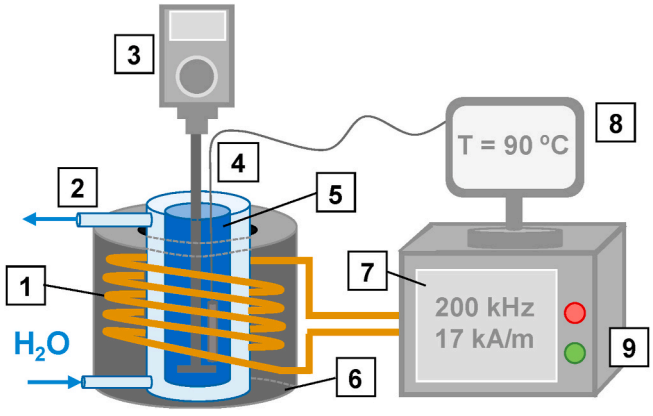

Scheme 1. Experimental set-up for SAR measurement and magnetic induction heating. (1) Inductor, (2) thermostat line, (3) mechanical stirrer, (4) temperature probe, (5) sample holder/reactor, (6) inductor insulator, (7) controller, (8) temperature indicator/recorder and (9) capacitors box.

quantify the amount of free radicals in the MNC, the EPR spectrum of the solution was recorded simultaneously with a pattern sample attached to the tube that hold the solution. This pattern sample corresponds to a MgO crystal doped with a known concentration of Mn^{2+} (Moreno Maldonado et al., 2019). The signal saturation effect for lower microwave attenuation was considered for the quantification.

The measured spectra were fitted using Bruker SPIN software, based on the hyperfine and g-factor parameters (Spin-Trap database of the National Institute of Environmental Health Sciences-NIEHS, USA, https://tools.niehs.nih.gov/stdb/index.cfm). The free-radical concentrations can be obtained by comparing the intensities of every specie in the EPR-fitted spectrum with the intensity of the MgO/Mn^{2+}, as previously reported (Davies, 2016; Raineri et al., 2019).

2.5. Adsorption experimentation

Room temperature adsorption experiments were carried out in a plastic 15 mL vial mixing 0.5 mL of the MNC (Fe concentration 10 mg/mL) and 9.5 mL of water sample with a specific concentration of pollutant. The mixture was mechanically stirred for a determined adsorption time and after equilibrium, the MNC was quickly separated (in 1 min) by means of a 60 × 30 mm NdFeB magnet with a 320 kA/m field gradient at the surface. The supernatant pollutant concentration in the aqueous phase was determined (C_e, mg/L) and the adsorption capacity was calculated considering Equation S2 (Aljerf, 2018).

Optimizing the adsorption conditions led us to analyze the effect of MNC dosage, from 5 to 25 mg, and the pH effect, between 2 and 6 for MO aqueous solutions, while for LIX and TIW the original pH (6 and 4) was maintained for industrial and application conveniences. It was also necessary a kinetic analysis of the adsorption at different times (5–1440 min) and at different initial concentrations (between 0 and 100 mg/L for MO, while for LIX and TIW the original sample was diluted four times). Data were fitted to pseudo-first order and pseudo-second order models, Langmuir and Freundlich isotherm models (Table S3). It was possible to estimate the maximum adsorption capacity, q_m (mg/g)(Gallo-Cordova et al., 2020).

2.6. Temperature and magnetic field assisted catalytic tests

The prepared MNC were tested in a series of AOP experiments for the degradation of organic compounds in MO aqueous solutions, TIW and LIX. All experiments were carried out in darkness at 30, 60 and 90 °C in a closed vessel. Degradation kinetics at different temperatures were performed at 550 rpm in an Eppendorf thermomixer comfort (Hamburg, Germany). Specifically, 5 mL of MNC (Fe concentration 10 mg/mL) were mixed with 45 mL of the MO aqueous solution (500 mg_{MO}/L), TIW (~500 mg_{cod}/L) and LIX (6560 mg_{cod}/L). Original TIW and LIX pH were maintained and MO pH was adjusted to 3 by addition of HNO_3 (pH values were controlled during the reaction). The MNC and water samples suspensions were mechanically stirred for 2 h to reach adsorption equilibrium. Then, to start the organic compounds degradation the optimum amount of H_2O_2 (where the entire reagent is consumed) was added to the suspension, corresponding to 0.051 M for MO and TIW, and 0.256 M for LIX in the final mixture. The decolorization kinetics were followed by taken aliquots (typically 2.5 mL) at certain times (0, 15, 30, 45, 60, 120 and 1440 min) and the MNC were magnetically separated from the media with the NdFeB magnet.

The enhancement of the AOP due to the magnetic heating was evaluated by conducting the reactions in 100 mL glass reactor adapted to the magnetic inductor (see Scheme 1) and under the application of an alternating magnetic field of 200 kHz and 17 kA/m, enough to reach 90 °C with the MNC as heating source. The effect of the AMF in the degradation of MO, TIW and LIX was compared to experiments carried out at 25, 60 and 90 °C heated with a conventional thermal reactor.

From the kinetic curve $C_t = f(t)$, it is possible to obtain the reaction rates by plotting the curve tangents at different times. From the variation of the supernatant concentrations at times 0 and 2 h, C_{2h} and C_0, the decolorization yield (DY) can be calculated ($DY = 100–100C_{2h}/C_0$). Mineralization was determined by analyzing the TOC in the supernatant calculated by $MY = 100–100[TOC]_{2h}/[TOC]_0$, where [TOC] is the total organic carbon at specific times (t = 0 and 2 h) (Ferroudj et al., 2013).

According to chemical kinetic theory, the chemical reaction rate is given by the reactants, like in this case the different pollutants and oxidative radicals. Depending on the reaction order, each degradation rate can be expressed as zero, first or second order. Table S4 shows the individual expression of each reaction order with their integrated form (Youssef et al., 2016).

3. Results and discussion

3.1. Synthesis and characterization of the magnetic nanocatalyst (MNC)

Solvothermal synthesis parameters were adjusted to produce MNCs with a multicore structure comprised of small iron oxide nanocrystals with a porous arrangement. The TEM picture displayed in Fig. 1a shows the high homogeneity of the MNCs as well as their multicore internal structure, consisting of small cores (~10 nm) aggregated in particles of 40 nm (σ = 0.13) (Fig. 1b). X-ray diffraction pattern confirms the typical inverse spinel structure of maghemite/magnetite as the only crystalline phase (Fig. 1c). Previous works on similar particles using Mössbauer spectroscopy have shown that the particles are mainly maghemite, a ferric oxide that is the oxidation product of magnetite (Gavilán et al., 2017). The width at half height of (311) reflection was selected to determine the size of the individual cores using Scherrer's equation. The crystal size obtained was 25 nm, confirming the polycrystalline structure of the MNCs. Previous studies indicate that crystal size could be larger than individual cores if the particles present epitaxial interfaces between the iron oxide cores (Hemery et al., 2017). MNCs dispersed in water formed a stable colloid with a Z-potential value of +17.7 mV at a pH of 3.5. The discrepancy observed between TEM size and hydrodynamic size (121 nm, PDI = 0.35) observed in DLS measurements (Fig. 1d) suggests a small aggregation degree of particles in the colloid, typically observed in relatively large magnetic nanoparticles.

The presence of DEG coating molecules on the surface MNC was analyzed by FT-IR and TGA (Fig. 1e and f). DEG is used in the synthesis of MNCs as solvent and reducing agent, but also as surfactant for the stabilization of the final product. The FT-IR spectrum displayed in Fig. 1e presents, together with the iron oxide lattice vibration bands (400-640 cm^{-1}) characteristic of the Fe-O bonds in the spinel structure, the typical DEG peak at 1666 cm^{-1} corresponding to of C=O stretching vibrations (Tao et al., 2011). The intense and narrow peak at 1380 cm^{-1} is generated by the nitrate byproducts produced during the acid treatment of MNCs, while the band at 3400 cm^{-1} corresponds to hydroxyl groups at particles' surface or from water molecules. The amount of organic material was estimated from TGA curves in Fig. 1f. Discarding the weight loss below 100 ºC, attributed to the evaporation of residual water molecules, the curve presents two main steps. The 3% of weight loss between 100 and 600 ºC is produced by the decomposition of DEG (around 250 ºC (Vasilakaki et al., 2018)). During the second step observed at temperatures over 600 ºC the mass decreases an additional 1%. Above this temperature, sintering and transformation of maghemite to hematite take place (DTA, Fig. 1f) (Cornell and Schwertmann, 2003).

Textural analyses of the MNC were performed to understand the materials porosity. N_2 adsorption-desorption isotherm and pore size distribution are shown in Fig. S1. The isotherm obtained for the MNC was clearly of type IV with an evidence of capillary condensation hysteresis loop (Thommes et al., 2015). The H4 loop matches perfectly to the MNC conformation as it is usually found in samples with aggregated crystals (Thommes et al., 2015). Table 1 summarizes the textural parameters of the MNC where an average pore diameter in the low range of mesopores (2–50 nm) can be observed. The highest pore volume was

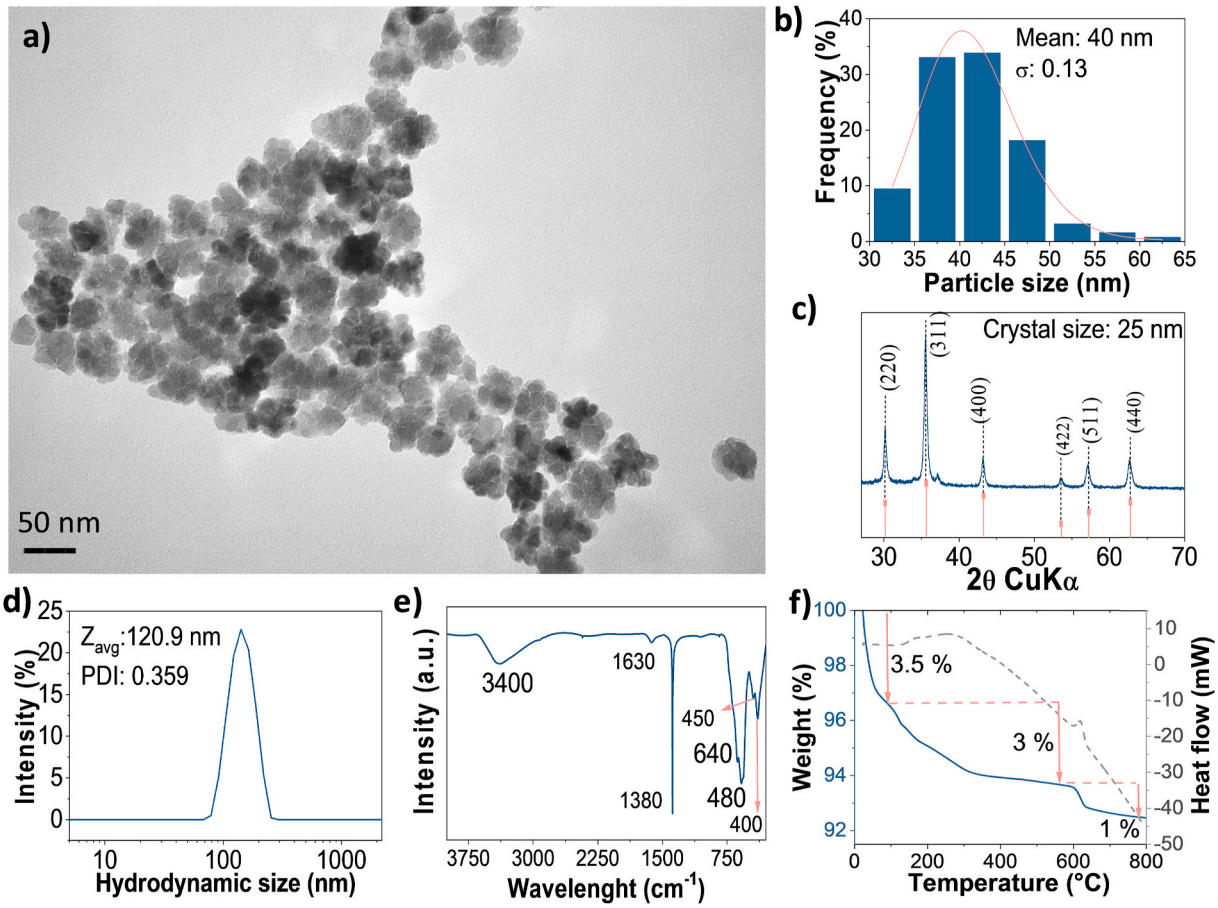

Fig. 1. Nanocatalyst structural characterization: a) TEM image, b) TEM size distribution, and log-normal fitting c) X-ray diffractogram, d) hydrodynamic size, e) FTIR transmittance spectrum and f) Thermogravimetric analysis.

obtained at approximately 4 nm.

The MNCs have interesting features for water remediation such as high surface to volume ratio and reactive surface, but also a strong magnetic response that can be exploited for the magnetic recuperation of the catalyst and the magnetically induced pollutant degradation. Fig. S2 shows the magnetophoresis performance of the MNC compared to single core nanoparticles of the same size by measuring the turbidity of the sample in a 2500 s time interval under a magnetic field gradient. The movement of the particles with higher magnetic moment per particle leads to a faster separation, exalting one of the advantages of using this engineered multicore catalyst for magnetic separation (Ovejero et al., 2017).

Fig. 2 shows the magnetic response of MNCs to quasistatic magnetic fields and magnetothermic response to high-frequency alternating magnetic field. The hysteresis loop in Fig. 2a presents the characteristic S-shape of the low-anisotropic monodomain response with a high saturation magnetization ($M_S = 80$ Am^2/kg) and susceptibility (4 Am^2/kg). The low coercivity observed ($H_C = 3$ kA/m) is due to the magnetic interactions presence between monodomains (superparamagnetic at room temperature if there were no interactions) and/or a little amount of larger particles presence (blocked at room temperature). The column bar chart in Fig. 2b shows the SAR obtained from the heating curves of the MNCs exposed to high frequency magnetic fields (100 and 200 kHz) at increasing field intensities. The maximum SAR value (850 W/g_{Fe}) was obtained at 200 kHz and 17 kA/m. It represents one of the highest values reported for iron oxide magnetic nanostructures (Nemati et al., 2018). In this case, the flower-like structure conformed by aggregates plays a fundamental role in the high SAR values due to a magnetic collective behavior between the cores within the particle. Nanoparticles aggregation can be controlled or tuned with the correct synthesis conditions improving magnetic properties (Gutiérrez et al., 2019; Ovejero et al., 2016).

Table 1
Nanocatalyst textural parameters.

BET area	*(m^2/g)*	35.875 ± 0.528
Average pore diameter	*(nm)*	9.981 ± 0.199
Pore volume	*(cm^3/g)*	0.044

Fig. 3a shows the typical EPR spectrum of the MNC in acetate buffer solution (pH = 5) containing the DMPO spin-trap and H_2O_2; measured at 24 °C, 30 min after the H_2O_2 was incorporated into the solution. The observed EPR spectra results from the convolution of the resonance signal of different paramagnetic species generated in the Fenton reaction plus the EPR signal of the MgO:Mn^{2+} pattern crystal (See Fig. S3). Each free radical presents a characteristic spectrum determined by the splitting of the resonance line due to the hyperfine interaction of the unpaired electron with the neighbor nucleus with non-null nuclear spins (I), as the H (I = 1/2) and N (I = 1). Based on the NIEHS Spin-Trap database, four different free radicals were clearly identified in the present Fenton reaction: •OH, •OOH, •CH_3, and •N. Table 2 shows the corresponding EPR parameters of each DMPO adducted free radicals; *i.e.* the g-factor of the free radicals, the hyperfine constants that quantify the interaction of the unpaired electron with the nitrogen (HS_N) and neighboring hydrogens (HS_H), the characteristic line width (W) and the lineshape (LS = 1 or 0 corresponds to a Lorentizan or Gaussian lineshape, respectively), of each resonance. The evolution of the Fenton reaction was followed by measuring the EPR spectrum as a function of time. All the spectra were fitted using the same set of parameters

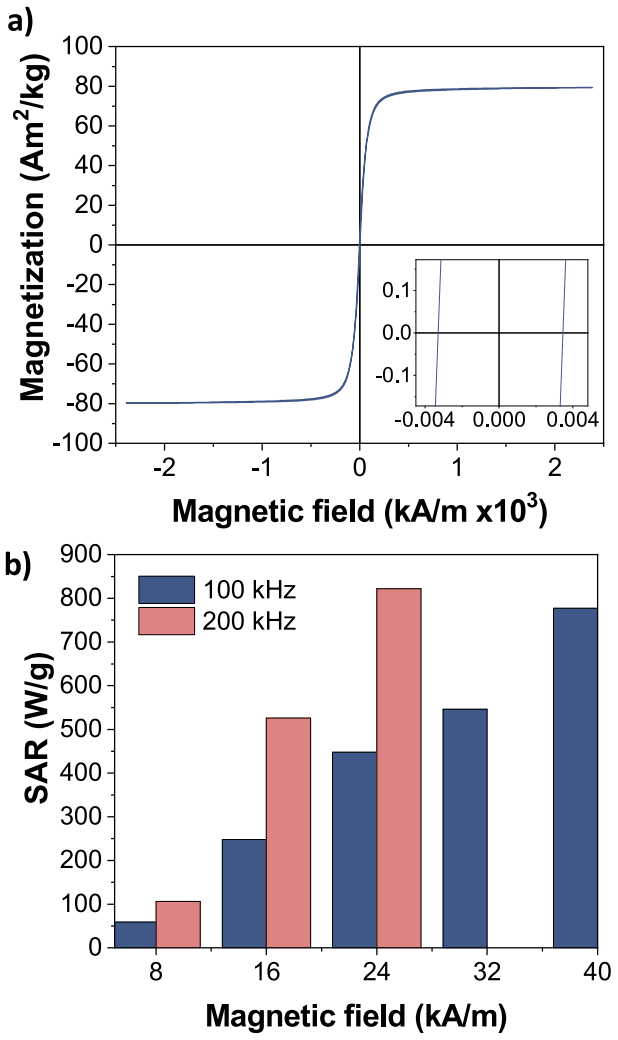

Fig. 2. a) Magnetic hysteresis loop of the MNC. b) SAR values of MNC at different AMF frequencies and fields intensities (all samples were measured at a concentration of 1 mg_{MNC}/mL).

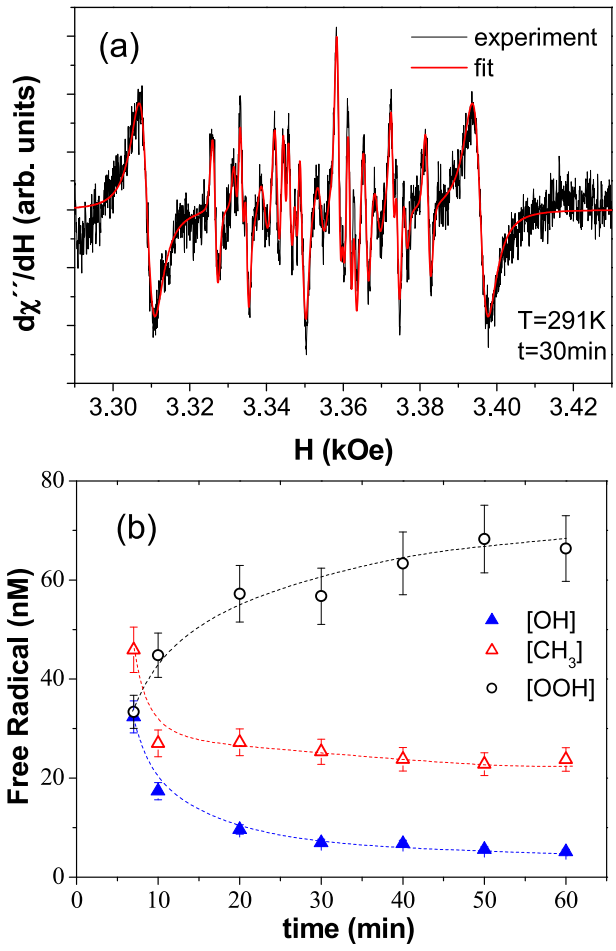

Fig. 3. a) EPR spectrum of MNC in DMPO/DMSO containing solution measured at 24 °C after 30 min of the addition of H_2O_2 and the corresponding fitting (See Fig. S3 for each subspectra component). b) Concentration of free radicals obtained from the fitting of the EPR spectra as a function of the time, the dashed lines are guides to the eye.

(Table 2), and only EPR intensity was varied for each free radical. It should be mentioned that the EPR intensity, obtained from the double integral of the spectrum, is proportional to the resonant paramagnetic specie concentration. Therefore, by comparing the EPR-fitted spectrum intensities of each species, •OH, •OOH, •CH_3, and •N, with the intensity of the MgO/Mn^{2+} pattern sample, it was possible to determine the free-radical concentration (Chang et al., 1978; Tobia et al., 2014). Fig. 3b shows the evolution of the free radical concentration as a function of time. As the concentration of the •N radical was very small compared to the other three species and it was present in the control solution without MNC, it was not considered in the discussion. The reaction stabilizes after 20 min, as observed in Fig. 3b. It should be clarified that the total hydroxyl radical concentration results from the contribution of the •OH signal and the •CH_3 signal, being the •CH_3 radicals formed as a consequence of the interaction between the •OH radical with DMSO. However, the •OOH radical was the main radical specie formed. This result is consistent with the larger proportion of Fe^{3+} on the MNC surface expected as a consequence of the nanoparticle surface oxidation with the acidic treatment.

The major role played by the Fe^{3+} in the production of ROS suggests a Fenton-like mechanism in which these highly oxidative species can be formed by the reaction of the Fe^{3+} with hydrogen peroxide and confirm the maghemite nature of this nanocatalyst. An advantage of working with a maghemite MNC based on Fenton-like mechanism is that it can be assured that the material does not suffer a chemical degradation (like in the case of magnetite) which can decrease their catalytic activity. These results are especially important in the design of MNC that can be magnetically collected and reused.

Table 2
EPR parameters, obtained from the fitting, of the Mn^{2+} and the free radicals generated in the Fenton reaction: g-factor; line width (W); line shape (LS = 1 or 0 corresponds to a Lorentzian or Gaussian lineshape, respectively). HS corresponds to the hyperfine interaction of the different species: HS_Mn of the Mn^{2+} ions of the crystal pattern (S = 5/2, I = 5/2), HS_N and HS_H correspond to the interaction between the unpaired electron of the free radical with of the nuclear spins of the nitrogen (I = 1) and neighboring hydrogen (I = 1/2) ions.

Parameter	MgO: Mn^{2+}	DMPO/ •OH	DMPO/ •CH_3	DMPO/ •OOH	DMPO/ •N
g-factor	2.0038	2.0027	2.0025	2.0028	2.0026
W	4.1	1.1	1.4	1.1	1.8
LS	0.02	0.73	0.74	0.30	0.98
HS_Mn	86.8	–	–	–	–
HS_N	–	14.9 (2)	16.2	14.1	14.7
HS_H$_\beta$	–	14.5 (2)	23.2	11.1	–
HS_H$_\gamma$	–	–	–	1.3	–

3.2. Adsorptive measurements

Even though the aim of this research is to perform AOP on industrial wastewaters, it is necessary to analyze the possible adsorption of

pollutants onto the MNC to distinguish the pollutant elimination by adsorption from the degradation process (AOP). It is important to evaluate the MNC maximum adsorption capacity at the equilibrium. The decrease of COD in LIX and TIW samples and MO removal was studied for a fixed dosage of MNC varying parameters such as adsorption time and initial concentration. In LIX and TIW samples, original pH value was maintained to avoid the expensive acidification and alkalinization of effluents to lower production costs. For MO, a pH value of 3 was selected as this is the usually reported value in literature (Gallo-Cordova et al., 2020). MNC dosage was analyzed for MO (Fig. S4) and it was observed an increment in the removal with the dosage, decreasing the adsorption capacity as it is inversely proportional to the MNC dosage.

The effect of adsorption time of MO, TIW and LIX (Fig. 4a, b and 4c) showed that the adsorption equilibrium was rapidly reached at 60, 20 and 120 min. Based on these results, a time of 120 min was established to ensure the equilibrium in the rest of adsorption and AOP experiments. It is important to determine the mechanism of adsorption and the kinetic model that better fits the experimental data, concluding what is the rate determining step: the reaction rate, mass transport or chemical reaction. Experimental data were best fitted to the pseudo-second order model in all three cases with a correlation factor $R^2 = 0.99$. With this information, it can be assumed that the rate-limiting stage of the adsorption process of MO, TIW and LIX is the surface adsorption. It means that pollutants removal process is mainly driven by its physicochemical interaction with the MNC surface (Gallo-Cordova et al., 2020).

The initial concentration effect was assessed by considering Langmuir and Freundlich isotherm models. The results of this experimentation are shown in Fig. 4d, e and 4f for MO, TIW and LIX. It can be observed from these figures that Langmuir model is able to describe the experimental data for the adsorption of pollutants in the wastewaters and MO onto the MNC. Accordingly, it can be assumed that the adsorption of the sorbate molecules is performed in a monolayer. Maximum adsorption capacity values were obtained with Langmuir model and where found to be 180 mg_{MO}/g for MO, 223 mg_{COD}/g for TIW and 320 mg_{COD}/g for LIX. The isotherms coefficients and kinetic constants can be found in Table S5.

3.3. Temperature and magnetic field-assisted oxidation

MO aqueous solution, as well as TIW and LIX samples were oxidized by oxidative radicals produced by the MNC catalyst in the presence of H_2O_2. The effect of H_2O_2 dosage, temperature and magnetic field were

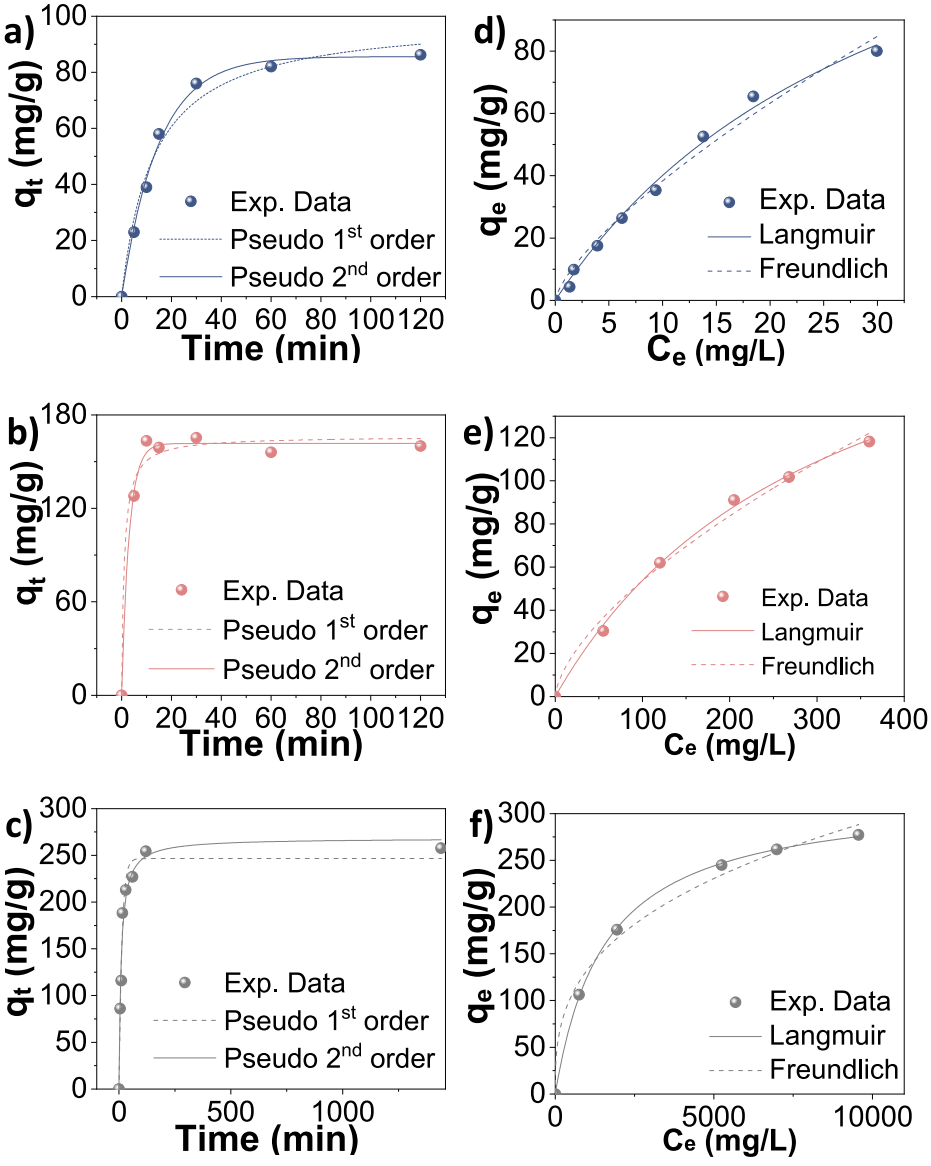

Fig. 4. Adsorption kinetic curves fit for a) MO b) TIW, c) LIX and isotherms for d) MO, e) TIW and f) LIX using MNC as adsorbent at room temperature.

analyzed for each pollutant in dark batch experimentation. The degradation kinetics were followed by COD measurements and the mineralization was determined by measuring the TOC of the samples after 2 h of reaction time. The decolorization of the samples was clearly temperature dependent as shown in Fig. 5a–c. It can be seen that for MO (Fig. 5a), the decolorization kinetic at room temperature was very efficient and slightly increased with increasing temperature, similarly to TIW (Fig. 5b).

A summary of the decolorization and mineralization yields is presented in Table 3. As it can be seen, at 90 °C decolorization yields achieved their maximum of 98.34 and 47.79% for MO and TIW, respectively. As expected, a complete decolorization of TIW was not reached, as this kind of wastewater with unknown composition usually presents certain compounds that cannot be degraded by AOPs, but they may be fully eliminated with a complementary biological treatment. Fig. 5c shows an impressive increase on the decolorization yield for LIX when elevating the temperature (up to 84.65% at 90 °C). When subjecting the MNC to an AMF, allowing the reaction to reach 90 °C, there was a slight increment in the decolorization of all samples and a much faster reaction, proving that even though the mixture is at the specified temperature, the MNC surface could reach higher temperatures improving the efficiency of the process. This would indicate a possible temperature gradient between the surface of the MNC and the sample media. Mineralization yields of the samples were calculated by measuring the TOC before and after the AOP. Fig. 5d displays the obtained results and it can be observed that, similarly to decolorization, TOC degradation increases with temperature for all samples and leads to higher yields under an AMF.

The obtained decolorization kinetics were adjusted to different reaction order models to understand the concentration dependence of the reaction rates. Regression analysis based on 0, 1st and 2nd order reactions for the degradation of MO, TIW and LIX were conducted. First order fittings maximized the regression coefficient value (R^2) presented in Table 3. In consequence, it can be concluded that the decolorization kinetics of MO, TIW and LIX are well described by first-order reactions. Apparent kinetic rate constants (k_1) described in Table 3 show that AMF reactions are much faster. For LIX, the reaction is 20% faster under the applied magnetic field than the reaction at 90 °C, going from a kinetic constant value of $(1.4)10^{-2}$ to $(1.7)10^{-2}$ min^{-1}.

Table 3
Decolorization (DY) and mineralization (MY) yields after 2 h through oxidation at 25, 60, 90 °C and in presence of an alternating magnetic field (AMF), apparent kinetic constants of first-order reaction and activation energy (E_a).

Temp.	DY	MY	k_1	n = 1	E_a
(°C)	(%)	(%)	(min^{-1})	R^2	(kJ/mol)
Methyl Orange (MO)					
25	92.20 ± 1.66	47.82 ± 4.53	$(1.8)10^{-2}$	0.983	18.42
60	98.31 ± 1.66	51.06 ± 4.46	$(2.9)10^{-2}$	0.981	
90	98.34 ± 1.66	62.96 ± 4.26	$(3.6)10^{-2}$	0.959	
90(AMF)	98.43 ± 1.66	68.23 ± 4.20	$(3.7)10^{-2}$	0.968	
Textile Industry Wastewater (TIW)					
25	41.38 ± 1.08	17.12 ± 0.49	$(3.9)10^{-3}$	0.969	4.39
60	45.17 ± 1.07	18.26 ± 0.49	$(4.4)10^{-3}$	0.998	
90	47.45 ± 1.06	22.97 ± 0.47	$(4.5)10^{-3}$	0.939	
90(AMF)	47.79 ± 1.18	24.09 ± 0.47	$(5.4)10^{-3}$	0.991	
Landfill Leachate (LIX)					
25	40.12 ± 0.03	37.39 ± 0.03	$(2.9)10^{-3}$	0.875	22.11
60	64.92 ± 0.02	45.84 ± 0.03	$(1.0)10^{-2}$	0.978	
90	84.65 ± 0.02	70.17 ± 0.02	$(1.4)10^{-2}$	0.991	
90(AMF)	90.21 ± 0.02	74.73 ± 0.02	$(1.7)10^{-2}$	0.999	

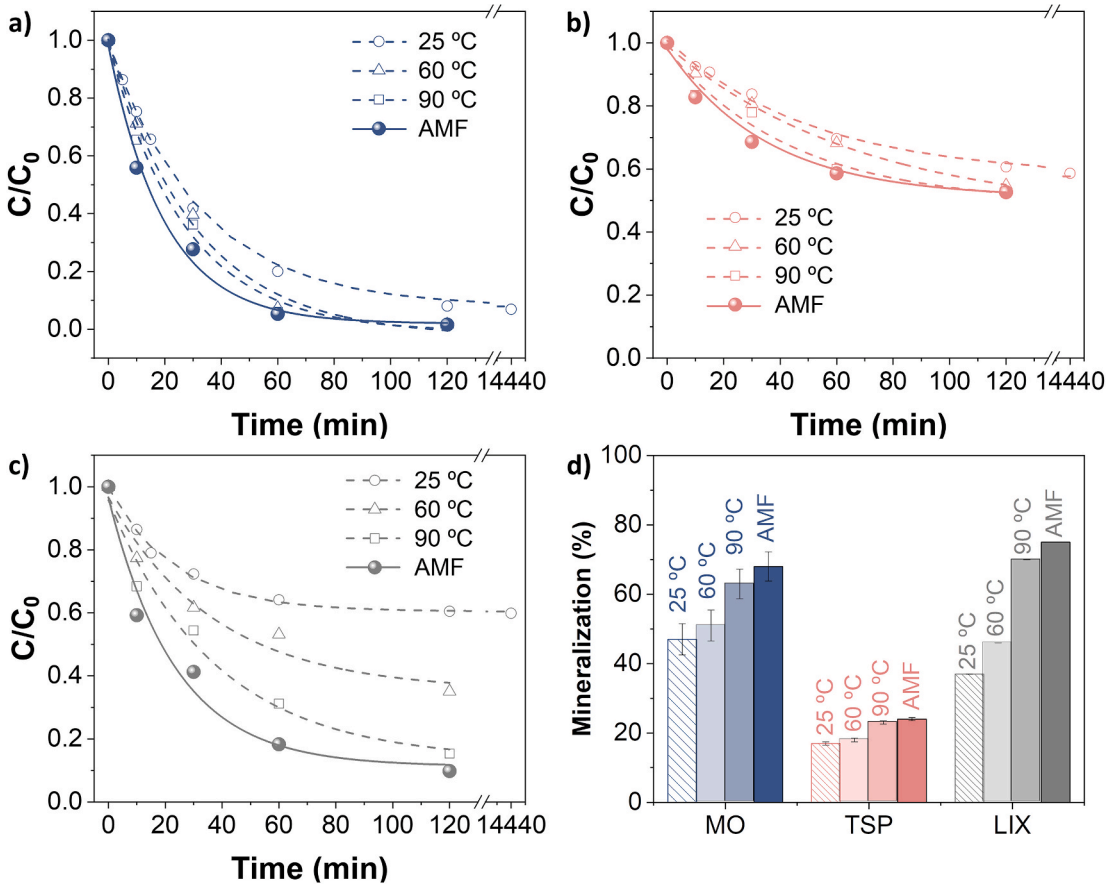

Fig. 5. Results of the advanced oxidation at 25, 60, 90 °C and in the presence of an alternating magnetic field (AMF): Decolorization kinetic curves of a) MO, b) TIW and c) LIX (errors are showed in Table 3). d) Mineralization yields at 2 h for MO, TIW and LIX.

The Arrhenius-type dependence of the kinetic constant k on the temperature and the activation energy values (E_a) are presented in Table 3. It can be seen that for MO a typical value of 18.42 kJ/mol was obtained in agreement with previous reported values (Shih et al., 2010), whereas for TIW and LIX, the values were 4.39 and 22.11 kJ/mol, which are difficult to compare with the bibliography since wastewater composition varies with location. It is important to highlight that these E_a values indicate the sensitivity of the reaction rate to temperature, which is in good agreement with the lower value for TIW.

The presented MNC is postulated as a very efficient catalyst for the magnetic field enhanced AOP of MO, TIW and LIX. This interesting way to accelerate reactions by taking advantage of the materials selective heating has not been deeply studied so far on real systems (Gallo--Cordova et al., 2021; Rivera et al., 2020). Table 4 shows the efficiency of different nanomaterials as catalysts in AOPs where it can be seen that just Chen et al. worked on dyes degradation considering the magnetic advantages of these materials (Chen et al., 2016). In that work, dye wastewater was treated in a high frequency inducting heating reactor showing an improvement in the reaction rate.

Analyzing the state of the art in this field, it can be concluded that the decolorization of MO is an easy achievable goal even at room temperature in very short times, supported by many reported data similar to the obtained results in this work (Jia et al., 2019; Mota et al., 2020; Youssef et al., 2016; Zhang et al., 2020). In the case of wastewater from textile industry TIW, it is difficult to compare with others works as this wastewater is specific of a local textile industry and its composition is the result of a mixture of the different effluents coming from the plant with high concentrations of NaCl, NaOH, as well as organic and organometallic dyes. The sample was obtained after treatment in a wastewater plant consisting of neutralizations step, followed by an aerobic bioreactor and a clarification process. Examining the bibliography, it was observed that dyes decolorization in aqueous solutions can be easily achieved when there is no interference with other compounds. In the case of real wastewaters from textile industries, their complex composition and the presence of reactive components obstruct a fully degradation with AOPs. However, treatment of leachate samples using nanocatalysts, independently on its nature, seems to be a very promising process showing very high efficiencies in the oxidation of the organic matter, like the results obtained in this work. The principal advantage of using magnetic nanocatalysts is that in the presence of an AMF, the catalysts can work as a heating source from inside the reactor. This approach improves the heating efficiency and reaches higher temperatures at the nanoparticle surface accelerating the degradation of the organic pollutants. Also, MNC can be easily recovered by magnetic separation allowing the reuse of the material.

With the presented AMF process, we achieved a total degradation of the MO compound, a reduction of approximate 6000 mg_{COD}/L for LIX and 250 mg_{COD}/L for TIW. In the latter cases, the final COD concentrations are still far from the 60 mg_{COD}/L that is considered the limit for discharge according to World Health Organization (WHO) (World Health Organization, 2006). However, the COD removed is considerable large and will facilitate further treatment processes, decreasing the efforts, costs and energy consumed in the global treatment process. As this kind of industrial wastewaters presents a complex composition (See Table S1 for the full description of the samples), it is possible that the full degradation of the samples was interfered by the presence of other elements such as phosphorous and aluminum in the samples (Fig. S5). Adsorption or ionic exchange of these compounds may be competing with the degradation. The concentration of iron in the samples before and after the AMF process was also measured by ICP-OES and a slight leaching of the MNC iron (4%) into the samples was detected. According to WHO the iron maximum permissible limit for discharge to streams is 5 mg/L (World Health Organization, 2006). It is important to acknowledge that the final iron concentration, in spite of its low toxicity, can contribute to soil acidification. As this degradation process is studied as a pretreatment for the samples, further treatment steps like low-cost filtration could be introduced for lowering the iron concentration (Khatri et al., 2017).

Besides the high efficiency of the process, it should be considered that wastewater treatment techniques must be sustainable from an environmental, ethical and economical point of view (Muga and Mihelcic, 2008). The presented treatment technique is a step forward for a more efficient heating that leads to better yields, shorter residence times and lower costs. An in-situ heating of the catalyst can provide a less consuming way of reaching operative temperatures on the catalyst surface or interphase, leading to a cleaner and cheaper production of unpolluted water. This water-energy nexus is a common and important mistreated issue (Capodaglio and Olsson, 2020).

4. Conclusion

In this work, an efficient iron oxide magnetic nanocatalyst has been developed and tested to improve the efficiency of organic matter advanced oxidation in leachate from a solid landfill and colored wastewater from a textile industry, proving for the first time the efficiency of this technology in real wastewaters. The use of this material presents great advantages against current treatment processes in terms of mass transfer limitations, energy consumption and catalyst separation. First, mass transfer limitations are decreased by using nanoparticles in suspension (colloids) due to the higher degree of mixing, higher amount of nanoparticles per volume and higher specific surface area. Then, we have proven that this catalyst can elevate reaction temperature (up to 90 °C at 1 mg/mL suspension in 5 min) by exposing it to an alternating magnetic field (17 kA/m, 200 kHz), in a more efficient

Table 4
Efficiency of different Fenton and Fenton-like catalysts on the decolorization and mineralization of different dyes and landfill leachates (NSF: not specified, N/C: not calculated).

Sample	Catalyst	A_{BET} (m^2/g)	Temp. (°C)	Magnetic parameters	Time (min)	DY (%)	MY (%)	Ref.
Methyl orange	Fe_2O_3 multicore nanoparticles	35.88	90	200 kHz, 17 kA/m	120	98.43	68.2	This work
Methyl orange	None	NSF	25	–	15	97.8	N/C	Youssef et al. (2016)
Methyl orange	Polysaccharide/Fe(III)-porphyrin	NSF	25	–	90	100	N/C	Mota et al. (2020)
Methyl orange	Hydrophilic Fe_3O_4 nanoparticles	NSF	80	–	20	100	N/C	Jia et al. (2019)
Methyl orange	Vanadium Titanium Magnetite	1.246	65	–	120	99.65	N/C	Zhang et al. (2020)
Textile wastewater	Fe_2O_3 multicore nanoparticles	35.88	90	200 kHz, 17 kA/m	120	47.79	24.1	This work
Dye wastewater	Carbon@Fe[5]	NSF	33	High frequency	60	98.39	N/C	Chen et al. (2016)
Methylene blue	α-Fe_2O_3-Co_3O_4	109.2	65	–	60	96.4	N/C	Hazarika et al. (2020)
Methyl red	Polysaccharide/Fe(III)-porphyrin	NSF	25	–	90	100	N/C	Mota et al. (2020)
Leachate	Fe_2O_3 multicore nanoparticles	35.88	90	200 kHz, 17 kA/m	120	90.21	74.7	This work
Leachate	None	NSF	30	–	120	85	N/C	Aygun et al. (2012)
Leachate	$CuFe_2O_4$	NSF	25	–	60	57	N/C	Karimipourfard et al. (2020)
Leachate	Fe_3O_4	NSF	25	–	100	84.7	68	Niveditha and Gandhimathi (2020a)
Leachate	FeMoPO	NSF	25	–	90	84.9	71	Niveditha and Gandhimathi (2020b)

manner than common heating methods. It has been measured that, due to the materials composition, there is an elevated production of highly oxidative species. All these outstanding characteristics were reflected in the magnetic field enhanced degradation and mineralization of organic compounds in the wastewater samples. We have shown that by taking advantage of this catalyst selective heating, we can improve reaction rates (up to 20% faster) and the already good performance (at RT) of this material. These results are a step-forward to develop these magnetic induction-driven techniques in an industrial scale that will help wastewater treatment processes develop in a more sustainable way. There are feasible ways to scale-up the production of this material, and it does not involve any harmful or toxic effect on the streams given that it can be recovered by simple magnetic separation. The use of this AOP with iron oxide magnetic nanocatalyst before a biological treatment and filtration could lead to a fully decontamination of the discharged effluent in an efficient and affordable way.

CRediT authorship contribution statement

Alvaro Gallo-Cordova: Conceptualization, Methodology, Validation, Formal analysis, Investigation, Writing – original draft. **Juan José Castro:** Investigation. **Elin L. Winkler:** Investigation, Formal analysis. **Enio Lima:** Investigation, Formal analysis. **Roberto D. Zysler:** Investigation, Formal analysis, Funding acquisition. **María del Puerto Morales:** Conceptualization, Writing – review & editing, Resources, Supervision, Project administration, Funding acquisition. **Jesús G. Ovejero:** Methodology, Writing – review & editing, Visualization, Supervision. **Daniela Almeida Streitwieser:** Writing – review & editing, Resources, Supervision, Funding acquisition.

Declaration of competing interest

The authors declare that they have no known competing financial interests or personal relationships that could have appeared to influence the work reported in this paper.

Acknowledgements

This research was funded by the Spanish Ministry of Economy and Competitiveness under grant MAT2017-88148-R (AEI/FEDER, UE) and Consejo Superior de Invetigaciones Cientít PIE- 201960E062. This study was also supported by the USFQ Collaboration Grant 2018 Nº 11197 and the USFQ PoliGrants 2018–2019 Nº 12501. E.W., E.L.Jr and R.D.Z. acknowledge Argentine governmental agency ANPCyT (Project No. PICT-2016-0288 and PICT-2018-02565) and UNCuyo (Project No.06/C527 and 06/C528) for the financial support. Authors want to also acknowledge Villacapria Cia. Ltda. and Textiles San Pedro for providing the wastewater samples.

Appendix A. Supplementary data

Supplementary data to this article can be found online at https://doi.org/10.1016/j.jclepro.2021.127385.

References

Adeleye, A.S., Conway, J.R., Garner, K., Huang, Y., Su, Y., Keller, A.A., 2016. Engineered nanomaterials for water treatment and remediation: costs, benefits, and applicability. Chem. Eng. J. 286, 640–662. https://doi.org/10.1016/j.cej.2015.10.105.

Aljerf, L., 2018. High-efficiency extraction of bromocresol purple dye and heavy metals as chromium from industrial effluent by adsorption onto a modified surface of zeolite: kinetics and equilibrium study. J. Environ. Manag. 225, 120–132. https://doi.org/10.1016/j.jenvman.2018.07.048.

Ammar, S., Fiévet, F., 2020. Polyol synthesis: a versatile wet-chemistry route for the design and production of functional inorganic nanoparticles. Nanomaterials 10, 1–8. https://doi.org/10.3390/nano10061217.

Aramyan, S.M., 2017. Advances in fenton and fenton based oxidation processes for industrial effluent contaminants control-A review. Int. J. Environ. Sci. Nat. Resour. 2 https://doi.org/10.19080/ijesnr.2017.02.555594.

Augugliaro, V., Litter, M., Palmisano, L., Soria, J., 2006. The combination of heterogeneous photocatalysis with chemical and physical operations: a tool for improving the photoprocess performance. J. Photochem. Photobiol. C Photochem. Rev. 7, 127–144. https://doi.org/10.1016/j.jphotochemrev.2006.12.001.

Aygun, A., Yilmaz, T., Nas, B., Berktay, A., 2012. Effect of temperature on fenton oxidation of young landfill leachate: kinetic assessment and sludge properties. Glob. Nest J. 14, 487–495. https://doi.org/10.30955/gnj.000835.

Bethi, B., Sonawane, S.H., Bhanvase, B.A., Gumfekar, S.P., 2016. Nanomaterials-based advanced oxidation processes for wastewater treatment: a review. Chem. Eng. Process. Process Intensif. 109, 178–189. https://doi.org/10.1016/j.cep.2016.08.016.

Brunauer, S., Emmett, P.H., Teller, E., 1938. Adsorption of gases in multimolecular layers. J. Am. Chem. Soc. 60, 309–319. https://doi.org/10.1021/ja01269a023.

Capodaglio, A.G., Olsson, G., 2020. Energy issues in sustainable urban wastewater management: use, demand reduction and recovery in the urban water cycle. Sustain. Times 12. https://doi.org/10.3390/su12010266.

Chang, T.T., Foster, D., Kahn, A.H., 1978. An intensity standard for electron paramagnetic resonance using chromium-doped corundum (Al_2O_3:Cr^{3+}). J. Res. Natl. Bur. Stand. 83, 133. https://doi.org/10.6028/jres.083.008.

Chen, H., Lee, J., Zheng, Y., Duan, Q., 2016. A non-traditional energy transfer process in CWPO heterogeneous reaction for wastewater treatment. Chem. Eng. Res. Des. 114, 142–147. https://doi.org/10.1016/j.cherd.2016.08.020.

Cornell, R.M., Schwertmann, U., 2003. The Iron Oxides: Structure, Properties, Reactions, Occurences and Uses. Wiley-VCH Verlag GmbH & Co. KGaA. https://doi.org/10.1002/3527602097.

Costo, R., Morales, M.P., Veintemillas-Verdaguer, S., 2015. Improving magnetic properties of ultrasmall magnetic nanoparticles by biocompatible coatings. J. Appl. Phys. 117, 1–7. https://doi.org/10.1063/1.4908132.

Davies, M.J., 2016. Detection and characterisation of radicals using electron paramagnetic resonance (EPR) spin trapping and related methods. Methods 109, 21–30. https://doi.org/10.1016/j.ymeth.2016.05.013.

Eaton, G.R., Eaton, S.S., Barr, D.P., Weber, R.T., 2010. Quantitative EPR. Springer-Verlag, Germany. https://doi.org/10.16309/j.cnki.issn.1007-1776.2003.03.004.

Ferroudj, N., Nzimoto, J., Davidson, A., Talbot, D., Briot, E., Dupuis, V., Bée, A., Medjram, M.S., Abramson, S., 2013. Maghemite nanoparticles and maghemite/silica nanocomposite microspheres as magnetic Fenton catalysts for the removal of water pollutants. Appl. Catal. B Environ. 136–137, 9–18. https://doi.org/10.1016/j.apcatb.2013.01.046.

Gallo-Cordova, A., Almeida Streitwieser, D., Morales, M.P., Ovejero, J.G., 2021. Magnetic iron oxide colloids for environmental applications. In: Colloids - Types, Preparation and Applications. Intech Open, pp. 1–25. https://doi.org/10.5772/intechopen.95351.

Gallo-Cordova, A., Lemus, J., Palomares, F.J., Morales, M.P., Mazarío, E., 2020. Superparamagnetic nanosorbent for water purification: assessment of the adsorptive removal of lead and methyl orange from aqueous solutions. Sci. Total Environ. 711, 134644 https://doi.org/10.1016/j.scitotenv.2019.134644.

Gallo-Cordova, A., Morales, M.P., Mazarío, E., 2019. Effect of the surface charge on the adsorption capacity of chromium(VI) of iron oxide magnetic nanoparticles prepared by microwave-assisted synthesis. Water (Switzerland) 11, 1–12. https://doi.org/10.3390/w11112372.

Gallo-Cordova, A., Veintemillas-Verdaguer, S., Tartaj, P., Mazarío, E., Morales, M.P., Ovejero, J.G., 2021. Engineering Iron Oxide Nanocatalysts by a Microwave-Assisted Polyol Method for the Magnetically Induced Degradation of Organic Pollutants. Nanomaterials 11 (4), 1052. https://doi.org/10.3390/nano11041052.

Garrido-Cardenas, J.A., Esteban-García, B., Agüera, A., Sánchez-Pérez, J.A., Manzano-Agugliaro, F., 2020. Wastewater treatment by advanced oxidation process and their worldwide research trends. Int. J. Environ. Res. Publ. Health 17. https://doi.org/10.3390/ijerph17010170.

Gautam, P., Kumar, S., Lokhandwala, S., 2019. Advanced oxidation processes for treatment of leachate from hazardous waste landfill: a critical review. J. Clean. Prod. 237, 117639 https://doi.org/10.1016/j.jclepro.2019.117639.

Gavilán, H., Kowalski, A., Heinke, D., Sugunan, A., Sommertune, J., Varón, M., Bogart, L. K., Posth, O., Zeng, L., González-Alonso, D., Balceris, C., Fock, J., Wetterskog, E., Frandsen, C., Gehrke, N., Grüttner, C., Fornara, A., Ludwig, F., Veintemillas-Verdaguer, S., Johansson, C., Morales, M.P., 2017. Colloidal flower-shaped iron oxide nanoparticles: synthesis strategies and coatings. Part. Part. Syst. Char. 34, 1–12. https://doi.org/10.1002/ppsc.201700094.

Gehrke, I., Geiser, A., Somborn-Schulz, A., 2015. Innovations in nanotechnology for water treatment. Nanotechnol. Sci. Appl. 8, 1–17. https://doi.org/10.2147/NSA.S43773.

Grace Pavithra, K., Senthil Kumar, P., Jaikumar, V., Sundar Rajan, P., 2019. Removal of colorants from wastewater: a review on sources and treatment strategies. J. Ind. Eng. Chem. 75, 1–19. https://doi.org/10.1016/j.jiec.2019.02.011.

Gutierrez, A.M., Dziubla, T.D., Hilt, J.Z., 2017. Recent advances on iron oxide magnetic nanoparticles as sorbents of organic pollutants in water and wastewater treatment. Rev. Environ. Health 32, 111–117. https://doi.org/10.1515/reveh-2016-0063.

Gutiérrez, L., De La Cueva, L., Moros, M., Mazarío, E., De Bernardo, S., De La Fuente, J. M., Morales, M.P., Salas, G., 2019. Aggregation effects on the magnetic properties of iron oxide colloids. Nanotechnology 30. https://doi.org/10.1088/1361-6528/aafbff.

Hach Co, 1999. U.S. Patent 6368870, Controlled Diffusion Analysis.

Hazarika, K.K., Hazarika, D., Bharali, P., 2020. Binary α-Fe_2O_3–Co_3O_4 nanostructures for advanced oxidation process: role of synergy for enhanced catalysis. Appl. Organomet. Chem. 1–11. https://doi.org/10.1002/aoc.5920.

He, J., Yang, X., Men, B., Wang, D., 2016. Interfacial mechanisms of heterogeneous Fenton reactions catalyzed by iron-based materials: a review. J. Environ. Sci. (China) 39, 97–109. https://doi.org/10.1016/j.jes.2015.12.003.

Hemery, G., Keyes, A.C., Garaio, E., Rodrigo, I., Garcia, J.A., Plazaola, F., Garanger, E., Sandre, O., 2017. Tuning sizes, morphologies, and magnetic properties of monocore versus multicore iron oxide nanoparticles through the controlled addition of water in the polyol synthesis. Inorg. Chem. 56, 8232–8243. https://doi.org/10.1021/acs.inorgchem.7b00956.

Hodges, B.C., Cates, E.L., Kim, J.-H., 2018. Challenges and prospects of advanced oxidation water treatment processes using catalytic nanomaterials. Nat. Nanotechnol. 13, 642–650.

ISO 5667-3:2019, 2019. Water Quality - Sampling - Part 3: Preservation and Handling of Water Samples.

Ito, S., Yamamoto, D., 2015. Structure of the methyl orange-binding site on human serum albumin and its color-change mechanism. Biomed. Res. 36, 247–252. https://doi.org/10.2220/biomedres.36.247.

Jia, X., Chen, X., Liu, Y., Zhang, B., Zhang, H., Zhang, Q., 2019. Hydrophilic Fe_3O_4 nanoparticles prepared by ferrocene as high-efficiency heterogeneous Fenton catalyst for the degradation of methyl orange. Appl. Organomet. Chem. 33, 1–12. https://doi.org/10.1002/aoc.4826.

Karimipourfard, D., Eslamloueyan, R., Mehranbod, N., 2020. Heterogeneous degradation of stabilized landfill leachate using persulfate activation by $CuFe_2O_4$ nanocatalyst: an experimental investigation. J. Environ. Chem. Eng. 8, 103426 https://doi.org/10.1016/j.jece.2019.103426.

Khandelwal, H., Dhar, H., Thalla, A.K., Kumar, S., 2019. Application of life cycle assessment in municipal solid waste management: a worldwide critical review. J. Clean. Prod. 209, 630–654. https://doi.org/10.1016/j.jclepro.2018.10.233.

Khatri, N., Tyagi, S., Rawtani, D., 2017. Recent strategies for the removal of iron from water: a review. J. Water Process Eng. 19, 291–304. https://doi.org/10.1016/j.jwpe.2017.08.015.

Kjeldsen, P., Barlaz, M.A., Rooker, A.P., Baun, A., Ledin, A., Christensen, T.H., 2002. Present and long-term composition of MSW landfill leachate: a review. Crit. Rev. Environ. Sci. Technol. 32, 297–336. https://doi.org/10.1080/10643380290813462.

Kong, Z., Li, L., Xue, Y., Yang, M., Li, Y.Y., 2019. Challenges and prospects for the anaerobic treatment of chemical-industrial organic wastewater: a review. J. Clean. Prod. 231, 913–927. https://doi.org/10.1016/j.jclepro.2019.05.233.

Lartigue, L., Hugounenq, P., Alloyeau, D., Clarke, S.P., Lévy, M., Bacri, J.C., Bazzi, R., Brougham, D.F., Wilhelm, C., Gazeau, F., 2012. Cooperative organization in iron oxide multi-core nanoparticles potentiates their efficiency as heating mediators and MRI contrast agents. ACS Nano 6, 10935–10949. https://doi.org/10.1021/nn304477s.

Madhav, S., Ahamad, A., Singh, P., Mishra, P.K., 2018. A review of textile industry: wet processing, environmental impacts, and effluent treatment methods. Environ. Qual. Manag. 27, 31–41. https://doi.org/10.1002/tqem.21538.

Malhotra, N., Lee, J.S., Liman, R.A.D., Ruallo, J.M.S., Villaflores, O.B., Ger, T.R., Hsiao, C.D., 2020. Potential toxicity of iron oxide magnetic nanoparticles: a review. Molecules 25, 1–26. https://doi.org/10.3390/molecules25143159.

Martínez-Huitle, C.A., Brillas, E., 2009. Decontamination of wastewaters containing synthetic organic dyes by electrochemical methods: a general review. Appl. Catal. B Environ. 87, 105–145. https://doi.org/10.1016/j.apcatb.2008.09.017.

Miao, L., Yang, G., Tao, T., Peng, Y., 2019. Recent advances in nitrogen removal from landfill leachate using biological treatments – a review. J. Environ. Manag. 235, 178–185. https://doi.org/10.1016/j.jenvman.2019.01.057.

Miklos, D.B., Remy, C., Jekel, M., Linden, K.G., Drewes, J.E., Hübner, U., 2018. Evaluation of advanced oxidation processes for water and wastewater treatment – a critical review. Water Res. 139, 118–131. https://doi.org/10.1016/j.watres.2018.03.042.

Moreno Maldonado, A.C., Winkler, E.L., Raineri, M., Córdova, A.T., Rodríguez, L.M., Troiani, H.E., Pisciotti, M.L.M., Mansilla, M.V., Tobia, D., Nadal, M.S., Torres, T.E., De Biasi, E., Ramos, C.A., Goya, G.F., Zysler, R.D., Lima, E., 2019. Free-radical formation by the peroxidase-like catalytic activity of MFe_2O_4 (M = Fe, Ni, and Mn) nanoparticles. J. Phys. Chem. C 123, 20617–20627. https://doi.org/10.1021/acs.jpcc.9b05371.

Mota, H.P., Quadrado, R.F.N., Burgo, T.A.L., Iglesias, B.A., Fajardo, A.R., 2020. Polysaccharide/Fe(III)-porphyrin hybrid film as catalyst for oxidative decolorization of toxic azo dyes: an approach for wastewater treatment. Arab. J. Chem. 13, 5923–5938. https://doi.org/10.1016/j.arabjc.2020.04.021.

Muga, H.E., Mihelcic, J.R., 2008. Sustainability of wastewater treatment technologies. J. Environ. Manag. 88, 437–447. https://doi.org/10.1016/j.jenvman.2007.03.008.

Munoz, M., Nieto-Sandoval, J., Serrano, E., De Pedro, Z.M., Casas, J.A., 2020. CWPO intensification by induction heating using magnetite as catalyst. J. Environ. Chem. Eng. 8, 104085 https://doi.org/10.1016/j.jece.2020.104085.

Nemati, Z., Alonso, J., Rodrigo, I., Das, R., Garaio, E., García, J.Á., Orue, I., Phan, M.H., Srikanth, H., 2018. Improving the heating efficiency of iron oxide nanoparticles by tuning their shape and size. J. Phys. Chem. C 122, 2367–2381. https://doi.org/10.1021/acs.jpcc.7b10528.

Niveditha, S.V., Gandhimathi, R., 2020a. Flyash augmented Fe_3O_4 as a heterogeneous catalyst for degradation of stabilized landfill leachate in Fenton process. Chemosphere 242, 125189. https://doi.org/10.1016/j.chemosphere.2019.125189.

Niveditha, S.V., Gandhimathi, R., 2020b. Mineralization of stabilized landfill leachate by heterogeneous Fenton process with RSM optimization. Separ. Sci. Technol. 1–10. https://doi.org/10.1080/01496395.2020.1725573, 00.

Oulego, P., Collado, S., Laca, A., Díaz, M., 2016. Impact of leachate composition on the advanced oxidation treatment. Water Res. 88, 389–402. https://doi.org/10.1016/j.watres.2015.09.048.

Ovejero, J.G., Cabrera, D., Carrey, J., Valdivielso, T., Salas, G., Teran, F.J., 2016. Effects of inter- and intra-aggregate magnetic dipolar interactions on the magnetic heating efficiency of iron oxide nanoparticles. Phys. Chem. Chem. Phys. 18, 10954–10963. https://doi.org/10.1039/c6cp00468g.

Ovejero, J.G., Velasco, V., Abel, F.M., Crespo, P., Herrasti, P., Hernando, A., Hadjipanayis, G.C., 2017. Colloidal Nanoparticle Clusters to produce large FePt nanocrystals. Mater. Des. 113, 391–396. https://doi.org/10.1016/j.matdes.2016.10.042.

Paździor, K., Bilińska, L., Ledakowicz, S., 2019. A review of the existing and emerging technologies in the combination of AOPs and biological processes in industrial textile wastewater treatment. Chem. Eng. J. 376, 120597 https://doi.org/10.1016/j.cej.2018.12.057.

Pirsaheb, M., Moradi, S., Shahlaei, M., Wang, X., Farhadian, N., 2019. Simultaneously implement of both weak magnetic field and aeration for ciprofloxacin removal by Fenton-like reaction. J. Environ. Manag. 246, 776–784. https://doi.org/10.1016/j.jenvman.2019.06.045.

Rai, H.S., Bhattacharyya, M.S., Singh, J., Bansal, T.K., Vats, P., Banerjee, U.C., 2005. Removal of dyes from the effluent of textile and dyestuff manufacturing industry: a review of emerging techniques with reference to biological treatment. Crit. Rev. Environ. Sci. Technol. 35, 219–238. https://doi.org/10.1080/10643380590917932.

Raineri, M., Winkler, E.L., Torres, T.E., Vasquez Mansilla, M., Nadal, M.S., Zysler, R.D., Lima, E., 2019. Effects of biological buffer solutions on the peroxidase-like catalytic activity of Fe_3O_4 nanoparticles. Nanoscale 11, 18393–18406. https://doi.org/10.1039/c9nr05799d.

Rekhate, C.V., Srivastava, J.K., 2020. Recent advances in ozone-based advanced oxidation processes for treatment of wastewater- A review. Chem. Eng. J. Adv. 3, 100031 https://doi.org/10.1016/j.ceja.2020.100031.

Renou, S., Givaudan, J.G., Poulain, S., Dirassouyan, F., Moulin, P., 2008. Landfill leachate treatment: review and opportunity. J. Hazard Mater. 150, 468–493. https://doi.org/10.1016/j.jhazmat.2007.09.077.

Rice, E.W., Baird, R.B., Eaton, A.D., 2017. Standard Methods for the Examination of Water and Wastewater. American Water Works Association. https://doi.org/10.1016/B978-0-12-382165-2.00237-3.

Rishikeshi, S.N., Joshi, S.S., Temgire, M.K., Bellare, J.R., 2013. Chain length dependence of polyol synthesis of zinc ferrite nanoparticles: why is diethylene glycol so different? Dalton Trans. 42, 5430–5438. https://doi.org/10.1039/c2dt32026f.

Rivera, F.L., Recio, F.J., Palomares, F.J., Sánchez-Marcos, J., Menéndez, N., Mazarío, E., Herrasti, P., 2020. Fenton-like degradation enhancement of methylene blue dye with magnetic heating induction. J. Electroanal. Chem. 114773 https://doi.org/10.1016/j.jelechem.2020.114773.

Rosa, J.M., Tambourgi, E.B., Vanalle, R.M., Carbajal Gamarra, F.M., Curvelo Santana, J. C., Araújo, M.C., 2020. Application of continuous H_2O_2/UV advanced oxidative process as an option to reduce the consumption of inputs, costs and environmental impacts of textile effluents. J. Clean. Prod. 246 https://doi.org/10.1016/j.jclepro.2019.119012.

Rusevova, K., Kopinke, F.D., Georgi, A., 2012. Nano-sized magnetic iron oxides as catalysts for heterogeneous Fenton-like reactions-Influence of Fe(II)/Fe(III) ratio on catalytic performance. J. Hazard Mater. 241–242, 433–440. https://doi.org/10.1016/j.jhazmat.2012.09.068.

Saini, R.D., 2017. Textile organic dyes: polluting effects and elimination methods from textile waste water. Int. J. Chem. Eng. Res. 9, 975–6442.

Shih, Y.H., Tso, C.P., Tung, L.Y., 2010. Rapid degradation of methyl orange with nanoscale zerovalent iron particles. Sustain. Environ. Res. 20, 137–143.

Tao, K., Song, S., Ding, J., Dou, H., Sun, K., 2011. Carbonyl groups anchoring for the water dispersibility of magnetite nanoparticles. Colloid Polym. Sci. 289, 361–369. https://doi.org/10.1007/s00396-011-2380-5.

Thommes, M., Kaneko, K., Neimark, A.V., Olivier, J.P., Rodriguez-Reinoso, F., Rouquerol, J., Sing, K.S.W., 2015. Physisorption of gases, with special reference to the evaluation of surface area and pore size distribution (IUPAC Technical Report). Pure Appl. Chem. 87, 1051–1069. https://doi.org/10.1515/pac-2014-1117.

Tkaczyk, A., Mitrowska, K., Posyniak, A., 2020. Synthetic organic dyes as contaminants of the aquatic environment and their implications for ecosystems: a review. Sci. Total Environ. 717, 137222. https://doi.org/10.1016/j.scitotenv.2020.137222.

Tobia, D., Winkler, E.L., Milano, J., Butera, A., Kempf, R., Bianchi, L., Kaufmann, F., 2014. Determination of Gd concentration profile in UO_2-Gd_2O_3 fuel pellets. J. Nucl. Mater. 451, 207–210. https://doi.org/10.1016/j.jnucmat.2014.03.054.

Usman, M., Cheema, S.A., Farooq, M., 2020. Heterogeneous Fenton and persulfate oxidation for treatment of landfill leachate: a review supplement. J. Clean. Prod. 256 https://doi.org/10.1016/j.jclepro.2020.120448.

Vasilakaki, M., Ntallis, N., Yaacoub, N., Muscas, G., Peddis, D., Trohidou, K.N., 2018. Optimising the magnetic performance of Co ferrite nanoparticles: via organic ligand capping. Nanoscale 10, 21244–24253. https://doi.org/10.1039/c8nr04566f.

Villarroel-Rocha, J., Barrera, D., Sapag, K., 2014. Introducing a self-consistent test and the corresponding modification in the Barrett, Joyner and Halenda method for pore-size determination. Microporous Mesoporous Mater. 200, 68–78. https://doi.org/10.1016/j.micromeso.2014.08.017.

Wang, S., 2008. A Comparative study of Fenton and Fenton-like reaction kinetics in decolourisation of wastewater. Dyes Pigments 76, 714–720. https://doi.org/10.1016/j.dyepig.2007.01.012.

Wang, W., Tuci, G., Duong-Viet, C., Liu, Y., Rossin, A., Luconi, L., Nhut, J.M., Nguyen-Dinh, L., Pham-Huu, C., Giambastiani, G., 2019. Induction heating: an enabling technology for the heat management in catalytic processes. ACS Catal. 9, 7921–7935. https://doi.org/10.1021/acscatal.9b02471.

World Health Organization, 2006. A compendium of standards for wastewater reuse in the eastern mediterranean region World health organization Regional Office for the

eastern mediterranean Regional Centre for environmental health activities CEHA. World Heal. Organ. 19.

Wydra, R.J., Oliver, C.E., Anderson, K.W., Dziubla, T.D., Hilt, J.Z., 2015. Accelerated generation of free radicals by iron oxide nanoparticles in the presence of an alternating magnetic field. RSC Adv. 5, 18888–18893. https://doi.org/10.1039/c4ra13564d.

Xu, P., Zeng, G.M., Huang, D.L., Feng, C.L., Hu, S., Zhao, M.H., Lai, C., Wei, Z., Huang, C., Xie, G.X., Liu, Z.F., 2012. Use of iron oxide nanomaterials in wastewater treatment: a review. Sci. Total Environ. 424, 1–10. https://doi.org/10.1016/j.scitotenv.2012.02.023.

Yaqoob, A.A., Parveen, T., Umar, K., 2020. Role of nanomaterials in the treatment of wastewater A review. Water 12, 1–30.

Youssef, N.A., Shaban, S.A., Ibrahim, F.A., Mahmoud, A.S., 2016. Degradation of methyl orange using Fenton catalytic reaction. Egypt. J. Pet. 25, 317–321. https://doi.org/10.1016/j.ejpe.2015.07.017.

Zaidi, N.S., Sohaili, J., Muda, K., Sillanpää, M., 2014. Magnetic field application and its potential in water and wastewater treatment systems. Separ. Purif. Rev. 43, 206–240. https://doi.org/10.1080/15422119.2013.794148.

Zhang, W., Tang, G., Yan, J., Zhao, L., Zhou, X., Wang, H., Feng, Y., Guo, Y., Wu, J., Chen, W., Yuan, N., Li, M., 2020. The decolorization of methyl orange by persulfate activated with natural vanadium-titanium magnetite. Appl. Surf. Sci. 509, 144886 https://doi.org/10.1016/j.apsusc.2019.144886.

Zhou, Yanbo, Lu, J., Zhou, Yi, Liu, Y., 2019. Recent advances for dyes removal using novel adsorbents: a review. Environ. Pollut. 252, 352–365. https://doi.org/10.1016/j.envpol.2019.05.072.